

Stochastic Siamese MAE Pretraining for Longitudinal Medical Images

Taha Emre, Arunava Chakravarty, Thomas Pinetz, Dmitrii Lachinov, Martin J. Menten, Hendrik Scholl, Sobha Sivaprasad, Daniel Rueckert, Andrew Lotery, Stefan Sacu, Ursula Schmidt-Erfurth, Hrvoje Bogunović, for the PINNACLE Consortium, for the Alzheimer's Disease Neuroimaging Initiative (ADNI)

Abstract—Temporally aware image representations are crucial for capturing disease progression in 3D volumes of longitudinal medical datasets. However, recent state-of-the-art self-supervised learning approaches like Masked Autoencoding (MAE), despite their strong representation learning capabilities, lack temporal awareness. In this paper, we propose STAMP (Stochastic Temporal Autoencoder with Masked Pretraining), a Siamese MAE framework that encodes temporal information through a stochastic process by conditioning on the time difference between the 2 input volumes. Unlike deterministic Siamese approaches, which compare scans from different time points but fail to account for the inherent uncertainty in disease evolution, STAMP learns temporal dynamics stochastically by reframing the MAE reconstruction loss as a conditional variational inference objective. We evaluated STAMP on two OCT and one MRI datasets with multiple visits per patient. STAMP pretrained ViT models outperformed both existing temporal MAE methods and foundation models on different late stage Age-Related Macular Degeneration and Alzheimer's Disease progression prediction

This work was supported in part by Wellcome Trust Collaborative Award (PINNACLE) Ref. 210572/Z/18/Z, and has received support from the European Union, EIC-2023-PATHFINDEROPEN-01 (I-SCREEN, grant no. 101130093). Funded by the European Union. Views and opinions expressed are however those of the author(s) only and do not necessarily reflect those of the European Union or European Innovation Council and SMEs Executive Agency (EISMEA). Neither the European Union nor the granting authority can be held responsible for them. For the purpose of open access, the author has applied a CC-BY public copyright licence to any author accepted manuscript version arising from this submission.

Taha Emre, Thomas Pinetz, Dmitrii Lachinov, and Hrvoje Bogunović are with the Institute of Artificial Intelligence, Center for Medical Data Science, Medical University of Vienna, Austria (taha.emre@meduniwien.ac.at, hrvoje.bogunovic@meduniwien.ac.at).

Arunava Chakravarty and Stefan Sacu are with the Department of Ophthalmology and Optometry, Medical University of Vienna, Austria.

Ursula Schmidt-Erfurth is with Ophthalmic Image Analysis Group (OPTIMA), Medical University of Vienna, Austria.

Martin J. Menten and Daniel Rueckert are with BioMedIA, Department of Computing, Imperial College London, London, United Kingdom, and Chair for AI in Healthcare and Medicine, Technical University of Munich, Munich, Germany.

Sobha Sivaprasad is with Moorfields National Institute for Health and Care Biomedical Research Centre, Moorfields Eye Hospital, London, United Kingdom, and Institute of Ophthalmology, University College London, London, United Kingdom.

Hendrik P.N. Scholl is with Department of Clinical Pharmacology, Medical University of Vienna, Vienna, Austria, and Pallas Kliniken AG, Pallas Klinik Zürich, Zürich, Switzerland, and European Vision Institute, Basel, Basel-Stadt, Switzerland.

Andrew Lotery is with Faculty of Medicine, University of Southampton, Southampton, Hampshire, United Kingdom.

Data used in preparation of this article were obtained from the Alzheimer's Disease Neuroimaging Initiative (ADNI) database (adni.loni.usc.edu). As such, the investigators within the ADNI contributed to the design and implementation of ADNI and/or provided data but did not participate in analysis or writing of this report. A complete listing of ADNI investigators can be found at: http://adni.loni.usc.edu/wp-content/uploads/how_to_apply/ADNI_Acknowledgement_List.pdf

which require models to learn the underlying non-deterministic temporal dynamics of the diseases.

Index Terms—Masked-Autoencoding, Variational-Inference, Self-supervised-learning, Disease Progression.

I. INTRODUCTION

Longitudinal medical images are routinely acquired in hospitals across multiple visits for each patient to track degenerative disease progression and inform clinical decisions. In ophthalmology, Age-related macular degeneration (AMD), a major contributor to vision loss and blindness [1], causes irreversible tissue damage with the severity steadily worsening over time, and is diagnosed using 3D optical coherence tomography (OCT) scans. Intermediate stage AMD (iAMD) may follow one of two pathways: neovascular AMD (wet-AMD) and Geographic Atrophy (GA) (Fig. 1 - 1st & 2nd rows), indicating multiple prognostic paths [2]. Moreover, progression to late stage wet-AMD can occur suddenly (Fig. 1 - 1st row), contributing to the uncertainty. Similarly, Alzheimer's disease (AD) is an irreversible, progressive neurodegenerative disorder and the leading cause of dementia. With approximately 50 million people affected worldwide [3], early and accurate detection is critical. While current treatments only address symptoms, volumetric brain MRI is widely used in clinical settings to identify early structural changes in patients with cognitively normal (CN) and mild cognitive impairment (MCI) diagnosis to make informed clinical decisions and understand the onset of dementia [4] (Fig. 1 - 3rd row).

The ability to forecast the future trajectory of disease progression from the current patient scan is crucial for personalized treatment [5]. It can help prioritize patients at increased risk of converting to the advanced stage through timely treatment and frequent monitoring [6], [7]. However, manual identification of high-risk patients is often subjective, tedious, and error-prone. Moreover, the high cost of diagnostic labeling in longitudinal data often leaves them in forecasting. This underscores the need to develop automated methods that can utilize unlabeled longitudinal medical datasets.

Self-supervised learning (SSL) aims to leverage available unlabeled data to learn meaningful features about disease. In the longitudinal setting, SSL methods learn to model temporal relationships by comparing images from different time points without relying on any human supervision. Although most existing longitudinal SSL methods make use of multiple visits as input for future forecasting, they ultimately

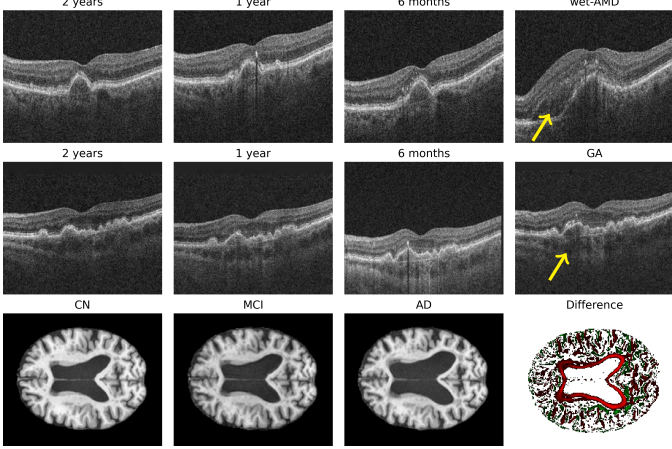


Fig. 1. **Top:** HARBOR dataset for wet-AMD conversion from iAMD, arrow pointing the subretinal fluid. **Middle:** PINNACLE dataset for GA conversion from iAMD, arrow pointing increasing light transmission due to atrophy. **Bottom:** ADNI dataset, CN to MCI to AD with difference map, red/green means decrease/increase in pixel intensity.

learn to extract deterministic temporal features. However, this is limiting because the rate of disease progression and the resulting anatomical changes vary significantly across patients. Therefore, it becomes crucial to model multiple possible future outcomes as a stochastic variable, allowing models to predict a distribution over a range of plausible disease progression trajectories. Leveraging large longitudinal medical datasets, we can model these temporal dynamics in an unsupervised manner so that future progression can be estimated from a single visit, reducing hospital load and enabling timely treatment planning.

In this work, we propose STAMP (Stochastic Temporal Autoencoder with Masked Pretraining), a novel SSL approach that extends masked auto-encoding to longitudinal medical imaging data within a Siamese framework. We hypothesize that latent factors driving temporal evolution can be inferred without explicit supervision by contrasting a patient’s two visits via a variational process. To account for the inherent uncertainty arising from these latent factors, we sample temporal feature tokens from a learned prior probability distribution conditioned on the time interval and the current input scan. STAMP is therefore able to capture long-term non-deterministic temporal dependencies using only two visits. Moreover, our SSL does not require spatio-temporal attention to learn temporal dynamics [8], making it model agnostic and compatible with standard Vision Transformer backbones. Our key contributions are¹:

- **Time Awareness:** We introduce a learnable encoding of time difference between input images, improving temporal image features over longer intervals.
- **Time-Conditioned Stochasticity:** We introduce a stochastic component into future image representations by sampling from a learned *time-conditioned* probability distribution, taking the uncertainty of the future into account.
- **3D Volumetric Extension:** We employ a fully 3D ap-

proach to learn representations of volumetric scans at each time point, marking the first adaptation of the Siamese MAE framework to 3D medical scans.

- **Extensive Evaluation:** We evaluate STAMP in two different modalities (OCT and MRI) on various prognostic tasks with different predictive time windows.

II. BACKGROUND AND RELATED WORK

Self-supervised learning is a pretraining approach that extracts meaningful representations from data without manual labels, thereby improving downstream performance when annotations are scarce. In medical imaging, SSL has been used for various downstream tasks, such as segmentation, disease classification, or disease forecasting [9]. Longitudinal medical datasets offer a unique opportunity to learn long-term relations with SSL. Previously, various longitudinal SSL methods have been developed using contrastive learning (temporal sensitivity [10], age as metadata [11]), and pretext learning (time difference prediction [12], patient-level trajectory modeling [13]). Although these models achieved considerable results, they are limited by metadata availability and large batch size dependency of contrastive learning [14], which makes scaling to longitudinal 3D volumes computationally inefficient.

However, with the advent of Vision Transformer (ViT) architectures, Masked Auto-encoding (MAE) [15] has emerged as the state-of-the-art SSL method for pretraining on unlabeled data. It addresses ViTs’ lack of inductive biases such as spatial locality and translation equivariance by adapting an image inpainting task [16] to the patch-based attention mechanism of ViTs. After dividing each input image into non-overlapping patches (*tokens*), MAE randomly masks up to 90% of them, and only the visible patches are processed by a ViT encoder to extract strong high- and low-level feature embeddings [17]. A lightweight ViT-based decoder then reconstructs the masked patches from the visible patch embeddings combined with learnable mask tokens and is trained with an L_2 loss. MAE has become the standard SSL pretraining step for a variety of domains, including medical imaging foundation models [18], [19]. Yet vanilla MAE-pretrained models lack the critical temporal information required for video or disease progression-based downstream tasks.

Longitudinal MAE has also been proposed for video datasets [20], [21] by stacking and masking frames to exploit temporal continuity and learn the temporal information between them. The longitudinal frames are treated as a volumetric input, and masking is done along both spatial and temporal dimensions. DropMAE [22] aims to improve upon [20] by dropping tokens from different frames that have high attention scores. This forces the network to use tokens from different frames, improving temporal reasoning. In comparison, longitudinal medical imaging data acquired across multiple patient visits presents unique challenges for SSL in general, and MAE in particular due to the temporal aspect involved in disease progression [23]. As a solution, these methods were adapted to medical images by stacking 2D scans from different time-points [24], [25] with longitudinal input specific model architectures. While these approaches improve

¹Source code is available at <https://github.com/EmreTaha/STAMP>

temporal tasks, they do not utilize cross-time completion to learn temporal relations, instead relying on stacking temporal images or frames to 3D inputs, which increases computation substantially and limits the inference to time-series input. In particular, stacking 3D medical volumes into 4D inputs further increases computational cost significantly.

Siamese Masked Autoencoders (SiamMAE) [26] improve temporal features using cross-time frame completion. It comprises two ViT encoders with shared weights (Siamese), and a cross-attention based decoder, reducing computational complexity. Two randomly sampled frames from a video are patchified and the future frame is masked similar to MAE. The encoder processes the unmasked past frame and the visible patches of the future frame. A learnable mask token is attached to each masked patch position in the future frame. The decoder performs cross-time completion by *querying* the visible patch embeddings and mask tokens, against the fully visible patch embeddings of the past frame, which provide the *Key* and *Value* for cross-attention. This allows network to reconstruct the future by comparing a fully visible past with a partially visible future, while improving computational efficiency compared to self-attention. After pretraining, the encoder is evaluated by feeding a single frame to predict the label of a future frame. Siamese MAE architecture is also used for temporal learning by mimicking the temporal changes via augmentation and reconstructing the augmented image [27] without temporal inputs. Similar Siamese MAE-based SSL has been used for 3D scene generation from 2D images of different angles [28], multi-scale representation learning [29] and camera depth estimation [30]. Although these methods leverage cross-time completion to learn temporal dynamics, their determinism limits them to modeling the mean behavior, preventing learning of multiple outcome scenarios.

While the deterministic SiamMAE captures temporal information efficiently, its deterministic nature fails when the future is fundamentally uncertain. In case of abrupt changes or progression, such as ball bouncing off a wall or the rapid AMD conversion to a late disease stage, these models tend to embed the average of possible outcomes, highlighting the need for stochasticity. As a pioneering work, Denton et al. [31] proposed to learn a stochastic prior from past frame embeddings to tackle the multi-outcome issue, removing the reliance on a fixed distribution used in Variational Autoencoders (VAE) [32]. The KL-divergence is computed between the learned prior and the posterior (derived from the future frame). Later on, it is adapted to ViT using stochastic tokens for action generation [33] by learning a stochastic prior token alongside the previous action embeddings in the attention blocks. Recently, RSP [34] introduced a learnable prior in SiamMAE pretraining for videos. The authors additionally proposed to learn a target distribution, denoted as posterior, which is derived from the past and future frames without masking to ensure a meaningful posterior distribution. The prior, which is only based on the past, is then aligned by penalizing the KL divergence between the two distributions [31], similar to the common practice in reinforcement learning [35]–[37]. Without masking, the model lacked the spatial knowledge, requiring another additional masked encoder pass to compensate,

increasing the computational cost substantially.

The aforementioned models incorporate stochasticity via time series input or multiple encoder passes, increasing computation and ambiguity in predictions as the time gaps grow. Especially RSP suffers from matching a time-independent prior to a time-dependent posterior which leads to time-insensitivity at inference and limits application to only close temporal proximity. As a result, these methods perform suboptimally on longitudinal medical data since intervals between patient visits can span several months or even years rather than seconds. This leads to two key differences between longitudinal medical images and natural videos: **(i)** longer intervals may require to explicitly encode the temporal information during representation learning; **(ii)** wide inter-subject variability in disease progression rates due to unknown latent factors (e.g. genetics, dietary habits) makes reconstruction of a single deterministic future state insufficient. STAMP addresses these points by reformulating SiamMAE as a time conditional variational inference. It directly learns a stochastic latent space conditioned on both the time interval and past embeddings, eliminating additional reconstruction tasks or the time unaware stochasticity as proposed in RSP.

III. METHODOLOGY

STAMP learns enhanced temporal features by improving future visit reconstruction of SiamMAE with conditioning on the time difference between two visit volumes and introducing stochasticity. The time difference conditioning also allows us to time-prompt the model during inference, which can be used for prognostic tasks with varying time windows solely using a single scan. In addition, to enable the network to model multiple possible future outcomes, we introduce time-conditioned stochasticity with a learned prior based on the past visit volume along with time difference and a posterior incorporating the future volume.

STAMP pretraining pipeline is depicted in Figure 2. The following sections describe and elaborate each step of the pipeline in order: **(1)** input and image masking, **(2)** temporal encoding, **(3)** stochasticity, **(4)** decoding (reconstruction), including **(5)** loss derivation.

1) 3D masking strategy: The longitudinal datasets consist of routinely monitored patients with 3D volumes $\mathbf{x} \in \mathbb{R}^{D \times H \times W}$ and \mathbf{x}_t denotes the scan acquired at visit date t from $\mathbb{T} = \{t \in \mathbb{N}_0; t \leq b\}$ with b being the last visit date. Then, from a patient, two visits are randomly sampled, yielding volumes \mathbf{x}_t and $\mathbf{x}_{t+\Delta t}$ with a time interval of $\Delta t \in \{n \in \mathbb{Z} \mid \Delta t_{min} \leq n \leq \Delta t_{max}\}$ between their acquisitions. Following the standard vision transformer pipeline, each volume is patchified using a 3D convolutional kernel [38], [39] (projection layer) into non-overlapping patches. In line with SiamMAE [26] for the SSL task of future reconstruction, 75% [18], [40] of $\mathbf{x}_{t+\Delta t}$ is masked, with the remaining visible patches denoted by $\tilde{\mathbf{x}}_{t+\Delta t}$. Fixed 3D sin-cos positional encodings are added to the patch embeddings of \mathbf{x}_t and $\tilde{\mathbf{x}}_{t+\Delta t}$. Finally, a learnable CLS token is appended to each input.

2) Temporal encoding (TE): We propose to incorporate time difference information using temporal encodings (TE)

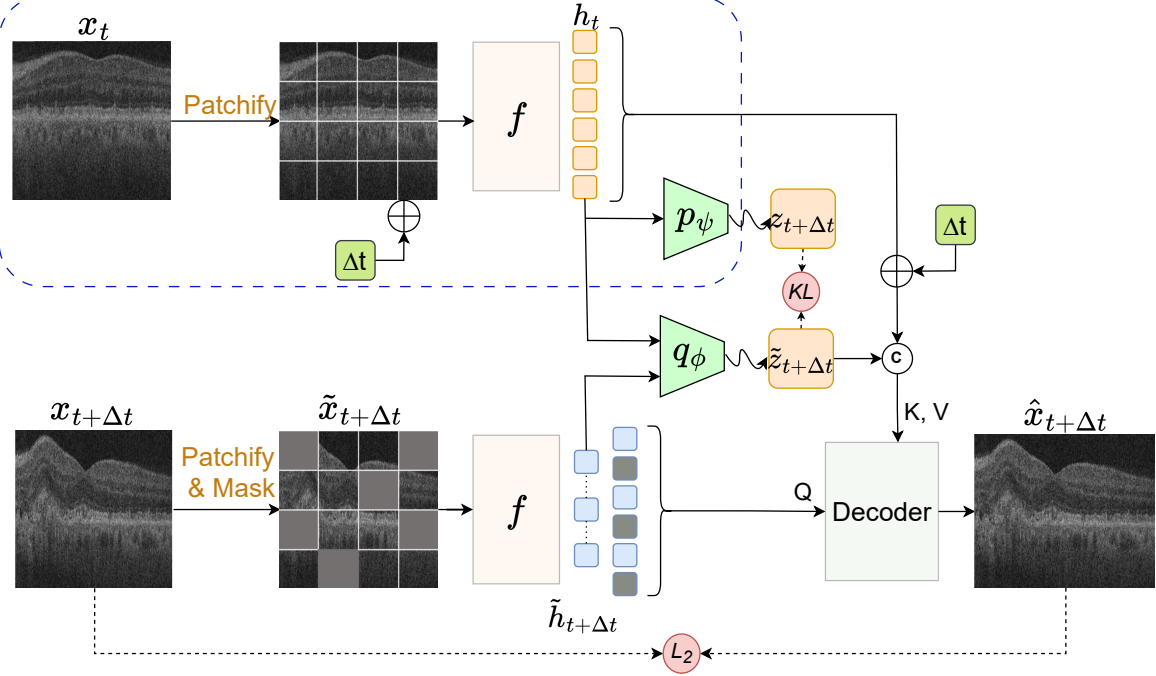


Fig. 2. An overview of STAMP. Two 3D volumes (x_t and $x_{t+\Delta t}$) Δt apart from a patient are used as input. After patchifying both scans, only the future visit is masked ($\tilde{x}_{t+\Delta t}$) and a learnable CLS token is attached to both branches. Δt and the subsequent summation indicate *TE* added to the CLS token in x_t branch. A ViT-based encoder f embeds the past visit and visible patches of the future into h_t and $\tilde{h}_{t+\Delta t}$. For the stochasticity, the posterior (q_ϕ) is learned from the embeddings CLS_t and $CLS_{t+\Delta t}$ of the partially visible future, while the prior (p_ψ) is learned from CLS_t and TE . After sampling ($\tilde{z}_{t+\Delta t}$) from the posterior q_ϕ , a cross-attention-based decoder queries $\tilde{h}_{t+\Delta t}$ against $[z_{t+\Delta t}, h_t]$ to reconstruct the future visit ($\hat{x}_{t+\Delta t}$). Once pretrained, the components within the dashed blue line are available during inference for the downstream task.

that are generated similar to diffusion step embedding with in-context setup [41]. *TE* is generated by a learnable 2-layer MLP following [41] with a SiLU non-linearity function [42], which takes a 1D sin-cos wave from discretized Δt as input and embeds it.

$$H = \frac{\text{dim(embedding)}}{2}, \quad \omega_i = \exp\left(-\ln(200) \frac{i}{H}\right) \quad (1)$$

$$\text{TE}(\Delta t) = \text{MLP}([\cos(\Delta t \omega_i), \sin(\Delta t \omega_i)]_{i=0}^{H-1}).$$

Then, *TE* is used similar to the positional encodings as an additive bias to the CLS token before the encoder, similar to [43]. To be able to prompt the decoder at the inference time, a second *TE* is added before the decoder. In both cases, *TE* is added to the previous visit's CLS_t token (Fig. 2). The token is referred as CLS token as it is the nomenclature, even though there is no supervised task in the STAMP pretraining. Finally, a ViT-based encoder f_θ embeds patch and CLS tokens as h_t and $\tilde{h}_{t+\Delta t}$ from x_t and partially masked $\tilde{x}_{t+\Delta t}$ in a Siamese setup.

3) *Stochasticity*: After the encoder, CLS_t and $CLS_{t+\Delta t}$ are used as stochasticity tokens similar to [33]. In the Siamese setup, during training, the network has 3 inputs: the fully visible past x_t , the masked future $\tilde{x}_{t+\Delta t}$, and the time difference Δt . At inference, the model will have access only to the past volume x_t and the time difference (Fig. 2 dashed area) for the future progression prediction. As the target for our prior, the posterior is constructed with access to both CLS tokens extracted from the past and the partially visible future volumes (CLS_t and $CLS_{t+\Delta t}$). This diverges from RSP, where a fully

visible future $x_{t+\Delta t}$ is used, because it has been shown that a fully visible future could lead to posterior collapse to the mode of the future [36].

STAMP solves this by masking the future, and constructing a time conditioned prior. We aim to learn a prior distribution $p_\psi(z_{t+\Delta t}|h_t, \Delta t)$ that approximates the posterior without access to the future scan, unlike VAEs that use a fixed Gaussian prior or RSP prior $p_\psi(z_{t+\Delta t}|h_t)$. We condition the prior [31], [34] on CLS_t and Δt . Two separate 2-layer MLPs with SiLU activation, p_ψ and q_ϕ (Fig 2), generate the prior and posterior distribution logits respectively. Following [35], the outputs of the MLPs are used as logits to one-hot categorical distributions to interpret them as probability distributions.

The proposed **Prior** retains the temporal information from the *TE* (added to CLS_t) which allows us to interpret the stochasticity as a conditional variational inference. On the other hand, the **Posterior** $q_\phi(\tilde{z}_{t+\Delta t}|h_t, \tilde{h}_{t+\Delta t})$ is aware of the partial future due to masking ($CLS_{t+\Delta t}$), contrary to RSP. The stochastic embedding (SE) $\tilde{z}_{t+\Delta t}$ is obtained by sampling from the posterior, which is concatenated as a token with h_t to be used in the decoder. Straight-through estimator [44] is used for sampling during the forward pass to ensure uninterrupted gradient flow. The operation is as follows (SG indicates stop-gradient operation and $p_\theta(x)$ indicates probabilities of the logits from the distribution definition):²

$$z \sim \text{OneHot}(p_\theta(x)), \quad \hat{z} = z + p_\theta(x) - \text{SG}(p_\theta(x)). \quad (2)$$

²Reparametrization trick for Categorical Distribution requires Gumbel-Softmax relaxation

4) *Decoding*: The transformer decoder p_ϕ is based on cross-self-attention [26] and aims to construct the masked patches of the future scan. The tokens $[\hat{z}_{t+\Delta t}, h_t]$ from the past visit are used as *Key* and *Value*, while the masked future tokens $\tilde{h}_{t+\Delta t}$ concatenated with learnable *[MASK]* tokens, are used as *Query* (Fig. 2 *Decoder*), unlike a self-attention only decoder where the future tokens $\tilde{h}_{t+\Delta t}$ only attends to itself. Before the decoder, the second *TE* is added to CLS_t , while the decoder positional encodings are added to both branches. The decoder output is used in the reconstruction loss for the masked patches.

5) *Loss function*: STAMP pretraining loss is based on VAE loss. VAEs use evidence lower bound (ELBO) loss to reconstruct realistic images and bring the posterior learned from the latent representation distribution to the prior from a fixed distribution (Gaussian) with the following formula (input image is indicated as x_t for consistency with STAMP):

$$\mathcal{L} = \mathbb{E}_{z_t \sim q_\phi} [\log p_\phi(x_t | z_t)] - \beta D_{KL}(q_\phi \| \mathcal{N}(0, I)) \quad (3)$$

Later, VAE was extended to condition the latent space on a class label to increase the likelihood of generating images belonging to the given class (CVAE) [45]. While the posterior q_ϕ is conditioned on both the input image x_t and the condition t , the prior is still a fixed distribution. The condition is added to both the encoder and the decoder. The ELBO loss is:

$$\mathcal{L} = \mathbb{E}_{z_t \sim q_\phi} [\log p_\phi(x_t | z_t, t)] - \beta D_{KL}(q_\phi(z_t | x_t, t) \| \mathcal{N}(0, I)) \quad (4)$$

Following from CVAE, STAMP adapts its loss to the Siamese setup with masking, where q_ϕ is conditioned on both x_t and $\tilde{x}_{t+\Delta t}$, the prior p_ψ is only informed from x_t and Δt . Since the sampled variable z is modeled as a latent variable of the disease development, we assume that there is a dependency between z and Δt , hence the ELBO becomes³:

$$\mathcal{L} = \mathbb{E}_{\hat{z}_{t+\Delta t} \sim q_\phi} \left[\underbrace{\log p_\phi(\hat{x}_{t+\Delta t} | \hat{z}_{t+\Delta t}, x_t, \tilde{x}_{t+\Delta t})}_{\text{reconstruction loss}} \right] - \beta D_{KL} \left[\underbrace{q_\phi(\hat{z}_{t+\Delta t} | x_t, \tilde{x}_{t+\Delta t}) \| p_\psi(z_{t+\Delta t} | x_t, \Delta t)}_{KL-\text{divergence}} \right] \quad (5)$$

The first term is the masked future reconstruction with MSE loss:

$$\mathcal{L}_{MSE} = \frac{1}{|\mathcal{M}|} \sum_{m \in \mathcal{M}} |\hat{x}_{t+\Delta t}^{(m)} - x_{t+\Delta t}^{(m)}|^2 \quad (6)$$

where m is an index from the list of masked patches \mathcal{M} .

The second term brings the prior distribution conditioned on the past scan and the future time-interval alone, closer to the posterior distribution which has access to both the past as well as unmasked parts of the future volume enabling it to learn meaningful temporal representations. During implementation, a symmetric KL-divergence loss with *stop-gradient* [35] was used for numerical stability. Hafner et al. [35] showed that stop gradient and larger bias for the posterior are crucial

³In the network implementation, \mathbf{a} as in the formula are the embeddings h

TABLE I
STATISTICS OF THE DATASETS. DISEASE PATHWAYS ARE DEFINED AS A
DETECTED CONVERSION DURING THE STUDY.

Dataset	Class	# of Patients	# of Visits	Interval (months)
HARBOR	pretraining	579	12770	
	iAMD→iAMD	431	8141	1.0 ± 1.0
	iAMD→wet-AMD	117	1967	
PINNACLE	iAMD→iAMD	451	4260	
	iAMD→GA	99	621	3.2 ± 3.3
ADNI	CN→CN	584	2665	
	MCI→MCI	569	2570	
	MCI (CN)→AD	358	2112	12.9 ± 8.5
	AD	332	1043	

for preventing posterior collapse. Similar regularization is employed in [34], [46]. The full implementation of D_{KL} is:

$$D_{KL} = 0.2 * KL \left[q_\phi \parallel SG(p_\psi) \right] + 0.8 * KL \left[SG(q_\phi) \parallel p_\psi \right] \quad (7)$$

IV. EXPERIMENTAL SETTING

Datasets The HARBOR⁴ dataset consists of 1076 patients (eyes) with AMD in different stages, with monthly OCT scans over a 24 month period using Cirrus OCT scanner. We split the data into two separate parts for pretraining and wet-AMD conversion downstream prediction task with 5% converted within 6 months (Table I HARBOR). We further divided the downstream data into 4 folds at the patient level for cross-validation and reported the average results. To evaluate under image domain-shift and an additional task, we employed an external dataset, part of the retrospective PINNACLE initiative [47], consisting of scans from Topcon device with labels for conversion to GA from iAMD, within 12 months (Table I PINNACLE). It contains 550 patients (eyes) with 4260 OCT scans of which 7% converted within 12 months. OCT spatial dimensions are resized to 448×448 , and we used the central 32 B-Scans (1.5 mm) as the volumetric input.

We also used the ADNI [48] cohort for 3D brain MRI experiments⁵. The subset we used has 9265 T1-weighted MRIs with 3344 CN, 4022 MCI, and 1899 AD cases from 1990 patients (Table I ADNI). Following [49], the preprocessing steps with the order are Bias Field Correction [50], skull stripping [51], rigid registration to the 1 mm isotropic MNI template [52] yielding $182 \times 218 \times 182$ sized images. Finally, a center crop of $128 \times 128 \times 128$ is applied. The downstream task data consists of the MCI diagnosed volumes evaluated for conversion to AD within 1-3 years as a binary label.

⁴NCT00891735. <https://clinicaltrials.gov/ct2/show/NCT00891735>

⁵Data used in the preparation of this article were obtained from the Alzheimer's Disease Neuroimaging Initiative (ADNI) database (adni.loni.usc.edu). The ADNI was launched in 2003 as a public-private partnership, led by Principal Investigator Michael W. Weiner, MD. The primary goal of ADNI has been to test whether serial magnetic resonance imaging (MRI), positron emission tomography (PET), other biological markers, and clinical and neuropsychological assessment can be combined to measure the progression of mild cognitive impairment (MCI) and early Alzheimer's disease (AD)

TABLE II

ABLATION FOR THE PROPOSED TEMPORAL (TE) AND STOCHASTIC () COMPONENTS DURING PRETRAINING AND THE DOWNSTREAM TASK. ROW 7 CORRESPONDS TO STAMP. IN THE PRETRAINING COLUMN, (X) INDICATES A METHOD WITHOUT THE COMPONENT. IN THE DOWNSTREAM COLUMN, (X) INDICATES A COMPONENT ADDED IN THE PRETRAINING BUT NOT USED IN THE DOWNSTREAM TASK

Pretraining		Downstream		6-months			12-months			
SE	TE	SE	TE	AUROC \uparrow	PRAUC \uparrow	BACC \uparrow	AUROC \uparrow	PRAUC \uparrow	BACC \uparrow	
1	X	✓	-	X	0.634 \pm 0.019	0.111 \pm 0.019	0.587 \pm 0.012	0.602 \pm 0.064	0.156 \pm 0.039	0.564 \pm 0.052
2	X	✓	-	✓	0.675 \pm 0.043	0.120 \pm 0.028	0.612 \pm 0.036	0.640 \pm 0.053	0.188 \pm 0.041	0.591 \pm 0.033
3	✓	X	X	-	0.637 \pm 0.048	0.100 \pm 0.017	0.592 \pm 0.028	0.601 \pm 0.038	0.138 \pm 0.011	0.571 \pm 0.033
4	✓	X	✓	-	0.627 \pm 0.033	0.088 \pm 0.015	0.579 \pm 0.016	0.602 \pm 0.028	0.134 \pm 0.012	0.561 \pm 0.024
5	✓	✓	X	✓	0.690 \pm 0.036	0.127 \pm 0.027	0.612 \pm 0.043	0.652 \pm 0.061	0.180 \pm 0.063	0.601 \pm 0.052
6	✓	✓	✓	X	0.639 \pm 0.031	0.108 \pm 0.022	0.592 \pm 0.064	0.594 \pm 0.034	0.128 \pm 0.027	0.545 \pm 0.050
7	✓	✓	✓	✓	0.700 \pm 0.047	0.140 \pm 0.042	0.615 \pm 0.049	0.671 \pm 0.057	0.200 \pm 0.066	0.607 \pm 0.042

Baselines STAMP pretraining is tested against MAE-based methods: MAE [15], SiamMAE [26], CropMAE [27] and RSP [34]. Additionally, we compared against common pretrained weights from ImageNet and, in the case of OCT datasets, MAE-pretrained OCT foundation models Ret-Found [18] and VisionFM [19]. Both models were pretrained on 2D B-scans of OCT volumes. Thus, we expanded the initial projection layer by inflating the convolutional kernel [53]. Then, we provided extensive ablation studies. We used AMD progression prediction task on two datasets for evaluation on frozen backbones. For the disease progression, only the future is relevant, thus we kept the Δt positive between pairs and only considered future OCT reconstructions. We also provided pretraining baseline comparisons on 3D MRIs from ADNI cohort for Alzheimer’s Disease progression.

Pretraining setting We used ViT-Base as the encoder (12 blocks with embedding dimension of 768). The decoder consists of 6 blocks of cross-attention self-attention pairs with an embedding dimension of 384. Following [35], CLS tokens are split into 32 dimensional bins to be used in the straight-through estimator for stochasticity. All methods were pretrained for 800 epochs, with a batch size of 96, a learning rate of $1e-4$, and a weight decay of $1e-2$ in AdamW [54]. OCT pairs are randomly sampled with a Δt of 3–18 months and a monthly discretization for TE. OCT inputs are size of $32 \times 448 \times 448$ and patchified into patches of $4 \times 32 \times 32$. In ADNI experiments, the MRIs are of size $128 \times 128 \times 128$ and patchified into patches of $16 \times 16 \times 16$. Δt is calculated with a discretization of 6 months. We used random horizontal flip, color jittering, and cropping. We found that horizontal flip is crucial for preventing the network from ignoring the future and reconstructing solely based on the past in line with the results reported by Eymaël et al. [27]. All experiments were run on a single NVIDIA A100 GPU.

Downstream task evaluation After pretraining, the models were evaluated with frozen backbones and employed pre-trained TE & SE, if available, for highlighting the contribution of each component. The task is a binary conversion prediction given a time window (6-12 months for HARBOR, 12 months for PINNACLE, 1-3 years for ADNI) with the Cross-Entropy loss. We used Attention Pooling [55], [56] as an alternative to linear evaluation. After obtaining the input features from the encoder, Attention Pooling consists of a single cross-

attention layer added with an additional CLS token to attend the patch embeddings relevant for classification without any non-linearity. All experiments were run for 200 epochs with Adam optimizer. Learning rates are set using grid-search over the validation splits. We reported results with area under the receiver operating characteristic (AUROC), area under the precision-recall curve (PRAUC), and balanced accuracy (BACC), which corresponds to the average recall of classes. While the random prediction baseline for AUROC and BACC is 0.5, in PRAUC it is proportional to the positive class ratio. The PRAUC baselines are: 0.05 for HARBOR 6 months, 0.11 for HARBOR 12 months, 0.07 for PINNACLE 12 months, 0.07 for ADNI 1 year and 0.18 for ADNI 3 years tasks.

V. RESULTS

A. Effect of Temporal Encoding and Stochasticity

We conducted ablation studies to show the importance of pretraining with temporal encodings and stochasticity. Until now, most SSL-based models discarded the extra components that are learned during the pretraining, focusing on the general representation quality. We hypothesized that these components learn meaningful latent factors that could be lost due to fine-tuning or just discarding. We, therefore performed the ablation in two folds: adding TE & SE during pretraining, and employing them during the downstream evaluation (Fig. 2 blue dashed area).

First, we added unconditional stochasticity on SiamMAE (Table II Row 3). If RSP [34] is simplified without its third encoder pass (alongside the second reconstruction) and with masking the future input, it would yield the same model. Compared to RSP (Table III), reducing the pipeline complexity and the number of loss terms, clearly improved the pretraining stability, as evidenced by improvements across all metrics and tasks. We tested the learned stochasticity by sampling a stochastic token (SE) from its unconditional prior $z_t \sim p_\psi(z_t|h_t)$, and concatenated it $([z_t, h_t])$ (Table II Row 4) during the downstream evaluation. Due to its prior being unaware of Δt , it led to a decrease in the performance, highlighting the need for a TE. Similarly, low performance of RSP confirms our hypothesis that long time-intervals typical of medical imaging require time conditioning. This is supported by SiamMAE outperforming RSP. Thus, it can be concluded

TABLE III

LINEAR EVALUATION OF WET-AMD CONVERSION PREDICTION ON PRETRAINED MODELS WITHIN TWO TIME-WINDOWS: 6 AND 12 MONTHS ON THE HARBOR DATASET. IMAGENET, VISIONFM AND RETFOUND ARE FULLY FINETUNED. THE RESULTS ARE REPORTED OVER 4-FOLDS

Model	6-months			12-months		
	AUROC \uparrow	PRAUC \uparrow	BACC \uparrow	AUROC \uparrow	PRAUC \uparrow	BACC \uparrow
VisionFM [19]	0.631 \pm 0.036	0.090 \pm 0.010	0.583 \pm 0.075	0.593 \pm 0.053	0.126 \pm 0.017	0.553 \pm 0.058
ImageNet	0.665 \pm 0.029	0.096 \pm 0.026	0.614 \pm 0.033	0.640 \pm 0.022	0.151 \pm 0.052	0.578 \pm 0.013
RetFound [18]	0.636 \pm 0.043	0.091 \pm 0.027	0.560 \pm 0.024	0.551 \pm 0.024	0.121 \pm 0.042	0.531 \pm 0.033
TC [10]	0.643 \pm 0.033	0.101 \pm 0.011	0.611 \pm 0.050	0.599 \pm 0.067	0.143 \pm 0.042	0.564 \pm 0.057
MAE [15]	0.620 \pm 0.027	0.087 \pm 0.014	0.562 \pm 0.025	0.602 \pm 0.056	0.137 \pm 0.033	0.531 \pm 0.029
SiamMAE [26]	0.666 \pm 0.022	0.108 \pm 0.016	0.606 \pm 0.024	0.638 \pm 0.038	0.161 \pm 0.036	0.590 \pm 0.038
CropMAE [27]	0.675 \pm 0.020	0.105 \pm 0.017	0.612 \pm 0.023	0.523 \pm 0.018	0.097 \pm 0.011	0.503 \pm 0.008
RSP [34]	0.580 \pm 0.035	0.084 \pm 0.025	0.532 \pm 0.026	0.540 \pm 0.044	0.113 \pm 0.032	0.521 \pm 0.033
STAMP	0.700 \pm 0.047	0.140 \pm 0.042	0.615 \pm 0.049	0.671 \pm 0.057	0.200 \pm 0.066	0.607 \pm 0.042

that stochasticity without conditioning increases ambiguity in the feature space, degrading the model’s performance.

Next, we introduced temporal encodings on top of SiamMAE during pretraining (Table II Row 1-2). If the trained weights were transferred to ViT3D for the downstream task without employing *TE* during the downstream evaluation (Table II Row 1), it actually underperformed compared to SiamMAE (Table III). We speculate that some of the temporal latent factors is learned by *TE*. To demonstrate this, during the inference we prompted the network with Δt of 6 and 12 months for each task using the pretrained *TE*. The performance gain (Table II Row 2) compared to not using *TE* (Table II Row 1) during the inference and SiamMAE supports our claim. Finally, the combination of aforementioned two components yields the proposed STAMP.

TABLE IV
LINEAR EVALUATION OF GA CONVERSION PREDICTION WITHIN A 12 MONTHS TIME WINDOW ON THE PINNACLE DATASET. THE MODELS ARE PRETRAINED WITH THE HARBOR DATASET. THE RESULTS ARE REPORTED OVER 5-FOLDS

Model	AUROC \uparrow	PRAUC \uparrow	BACC \uparrow
TC [10]	0.770 \pm 0.058	0.150 \pm 0.054	0.702 \pm 0.046
MAE [15]	0.830 \pm 0.025	0.208 \pm 0.042	0.752 \pm 0.046
SiamMAE [26]	0.833 \pm 0.036	0.229 \pm 0.053	0.755 \pm 0.040
CropMAE [27]	0.818 \pm 0.026	0.174 \pm 0.041	0.744 \pm 0.023
RSP [34]	0.769 \pm 0.031	0.155 \pm 0.036	0.690 \pm 0.039
STAMP	0.848 \pm 0.020	0.240 \pm 0.061	0.769 \pm 0.047

B. AMD Progression

STAMP pretraining with TE & SE employed in the downstream tasks (Table III & Table II Row 7), outperformed the baselines and all ablation studies across all metrics, indicating its ability to learn multi-outcome temporal features. Even if SE is not employed during the linear evaluation (Table II Row 5), it outperformed the other methods, underscoring the quality of the pretraining phase. In Table IV, we used the pretrained weights from the HARBOR dataset for predicting GA conversion task on the PINNACLE dataset. STAMP achieved the best performance compared to the baselines, highlighting its feature robustness to image domain shift.

Additionally, we included available foundation models, namely VisionFM [19] and RetFound [18]. Both models failed to train when linearly evaluated, thus we fine-tuned them end-to-end. Although they performed better than linearly evaluated MAE, their lack of temporal information and possible domain shift due to scanner type or patient demographics, caused them to underperform significantly compared to STAMP (Table III).

Temporal sensitivity and sampling diversity of the learned prior are visualized in Figure 3. In the left, we sampled 20 tokens using the prior for each Δt . The resulting trajectories align correctly with increasing time intervals, demonstrating that both the temporal encoder (TE) and the prior capture time sensitivity. This observation is in line with the performance gap between STAMP and STAMP without SE (Table II Row 5). Moreover the principal component analysis (PCA) projection demonstrates that the prior distribution did not collapse to a single point, and was able to sample diverse and meaningful representations. To complement Figure 3, we visualized the change in attention scores with different *TE* (Fig 4). The images indicate the highest activating regions w.r.t CLS_t . It can be observed that if *TE* is removed from the encoder, the attention scores are more diffused around the image (Fig 4 Left), while with *TE* they are more focused (Fig 4 Middle & Right) on the retina. Another observation is that with different *TE* prompting, 3D locations of the highest attention scores changed. This is inline with the temporal sensitivity of the representations.

Also we evaluated the representation space under irregular time points by sampling with discrete (monthly), and fractional (every 15 days) time steps. Even though the model has never been trained with fractional time conditioning, in Figure 3 Right, it can be seen that the sampled tokens conditioned on fractional TE, follow the same time sensitive distribution. In Figure 5, TE values themselves are visualized with PCA. The fractional TEs deviate only slightly from the linearly interpolated values (in red).

Finally, computational overhead for each method is presented in Table V. STAMP has insignificant computational overhead compared to SiamMAE. While RSP is more computationally expensive with 3 forward passes from its encoder, over long time windows of medical datasets, it performance

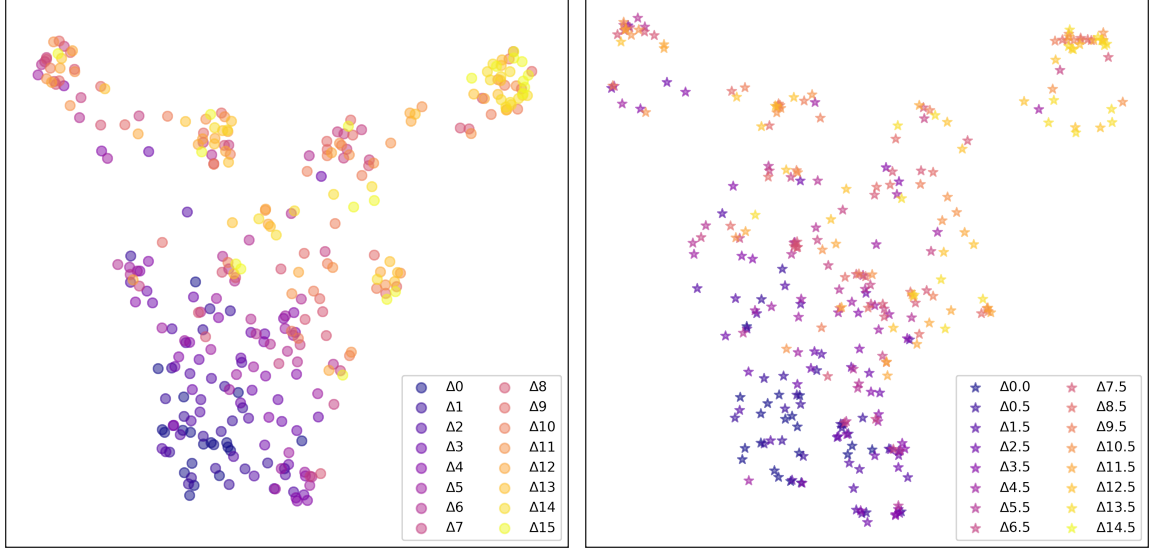


Fig. 3. **Left:** PCA projection of 20 sampled tokens from the learned prior p_ψ per discrete Δt . **Right:** PCA projection of 20 sampled tokens from the learned prior p_ψ per fractional Δt . The temporal alignment indicates diverse but time sensitive stochastic sampling in both cases.

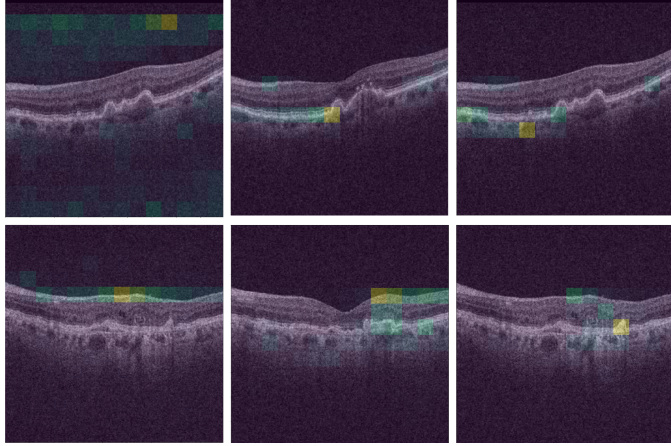


Fig. 4. Attention map visualization of STAMP w.r.t pretrained CLS. Each row is from a different volume. **Left:** Attention maps without using TE. **Middle:** Attention maps with 3 months prompted TE. **Right:** Attention maps with 15 months prompted TE.

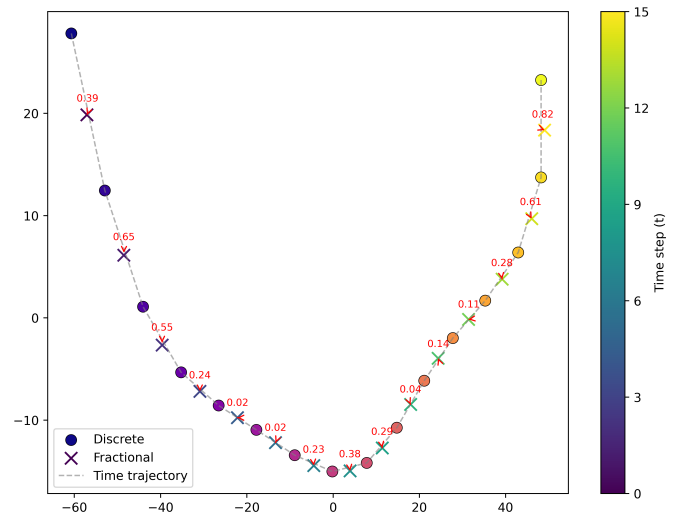


Fig. 5. PCA of TE per discrete (●) and fractional (X) Δt . The number indicates deviation of a fractional from the interpolated value between the discrete TEs.

TABLE V
NUMBER OF PARAMETERS AND FLOP PER ITERATION OF PRETRAINING

Model	GFLOP	# of Params (M)
MAE [15]	45.1	104.8
SiamMAE [26]	153.6	109.6
CropMAE [27]	153.6	109.6
RSP [34]	281.9	116.1
STAMP	153.7	117.4

drops considerably. On the other hand STAMP with simplified pipeline and time difference conditioning offers to pretrain the same ViT backbone better in a cost efficient manner.

C. AD Progression

We applied STAMP to 3D brain MRI using the ADNI dataset with irregular inter-visit time intervals across more than 60 centers (Table I), unlike HARBOR. Similar to the AMD progression prediction setup, the extracted features were linearly evaluated for AD progression prediction from MCI within 1 and 3 years (Table VI). Compared to AMD progression, ADNI evaluations highlight the generalizability of STAMP to different modalities, irregular visit schedules, and longer time windows. STAMP clearly outperformed other MAE based methods and a metadata-aware contrastive method [11] in 1 year task across all three metrics. It achieved competitive results for 3-year prediction task in terms of AUROC and PRAUC, while achieving the highest PRAUC,

TABLE VI

LINEAR EVALUATION OF AD CONVERSION PREDICTION ON PRETRAINED MODELS WITHIN TWO TIME WINDOWS: 1 AND 3 YEARS ON THE ADNI DATASET. THE RESULTS ARE REPORTED OVER REPEATED EXPERIMENTS

Model	1-year			3-years		
	AUROC \uparrow	PRAUC \uparrow	BACC \uparrow	AUROC \uparrow	PRAUC \uparrow	BACC \uparrow
Random init	0.690 \pm 0.006	0.142 \pm 0.002	0.628 \pm 0.010	0.713 \pm 0.030	0.317 \pm 0.039	0.652 \pm 0.015
ImageNet	0.736 \pm 0.007	0.188 \pm 0.013	0.639 \pm 0.008	0.712 \pm 0.041	0.301 \pm 0.056	0.670 \pm 0.024
yAware [11]	0.730 \pm 0.001	0.188 \pm 0.001	0.625 \pm 0.009	0.716 \pm 0.004	0.306 \pm 0.004	0.629 \pm 0.004
MAE [15]	0.721 \pm 0.002	0.152 \pm 0.002	0.634 \pm 0.012	0.712 \pm 0.002	0.285 \pm 0.004	0.674 \pm 0.011
SiamMAE [26]	0.775 \pm 0.004	0.220 \pm 0.001	0.721 \pm 0.006	0.787 \pm 0.001	0.362 \pm 0.003	0.726 \pm 0.002
CropMAE [27]	0.769 \pm 0.004	0.198 \pm 0.001	0.712 \pm 0.002	0.764 \pm 0.001	0.394 \pm 0.001	0.683 \pm 0.002
RSP [34]	0.785 \pm 0.002	0.215 \pm 0.002	0.723 \pm 0.009	0.738 \pm 0.002	0.339 \pm 0.004	0.671 \pm 0.004
STAMP	0.812 \pm 0.001	0.277 \pm 0.004	0.736 \pm 0.009	0.773 \pm 0.001	0.416 \pm 0.013	0.691 \pm 0.001

which is particularly important metric in the setting of class imbalance. Moreover, the lower performance of yaware [11] relative to temporal MAE [26], [27], [34], further underscores the representation quality of MAE over contrastive approaches.

VI. DISCUSSION & CONCLUSION

We introduce STAMP, a self-supervised framework that learns temporal dynamics through time-conditioned stochasticity, enabling accurate disease progression prediction across different modalities and prognostic horizons with limited labels. By extending Siamese MAE pretraining with a time difference conditioned learnable prior and a future-aware posterior, STAMP effectively formulates forecasting as conditional variational inference to address the challenging aspects of disease progression prediction: long visit intervals, varying progression speeds, and multiple potential outcomes. The stochasticity and the time conditioning make it possible to prompt the model for possible futures at inference time, using a single scan and a specified time window.

We pretrained STAMP on two longitudinal datasets: 3D OCT scans for AMD and MRI scans from the ADNI cohort for Alzheimer’s disease onset. We evaluated pretrained models across multiple prognostic windows using the pretrained temporal encoding and stochastic sampling. After pretraining STAMP on HARBOR, STAMP consistently outperformed existing baselines and foundation models on 6 and 12 months progression for wet-AMD (HARBOR) and 12 months GA progression (PINNACLE) as a domain shift experiment. Similarly, on ADNI MRI (1 and 3 years AD onset), STAMP surpassed both MAE based and age-aware pretraining models, demonstrating robustness under irregular visit intervals and extended prediction windows.

Although STAMP significantly advances MAE, its reliance on only two visit volumes during pretraining limits its ability to capture complex dynamic relationships. Pretraining on more than two volumes could further enhance its temporal capability; however it demands substantial computational resources for processing longitudinal 3D volumes. Moreover, the downstream task performance can be increased by predicting the onset with multiple visits, it would undermine the strengths of our model which is predicting the progression from a single visit utilizing the learned temporal and stochastic components.

Additionally, the prior’s large sampling space makes post hoc explainability analysis of the sampled tokens challenging.

Clinically, STAMP helps with utilizing large unlabeled datasets to improve personalized monitoring by forecasting individual disease trajectories from a single baseline scan, facilitating tailored follow-up schedules, earlier intervention for high-risk patients, and reducing hospital load. This demonstrates the promise of self-supervised, time-conditioned stochastic modeling for advancing precision medicine in progressive diseases.

APPENDIX A ACKNOWLEDGMENT

Data collection and sharing for this project was funded by the Alzheimer’s Disease Neuroimaging Initiative (ADNI) (National Institutes of Health Grant U01 AG024904) and DOD ADNI (Department of Defense award number W81XWH-12-2-0012). ADNI is funded by the National Institute on Aging, the National Institute of Biomedical Imaging and Bioengineering, and through generous contributions from the following: AbbVie, Alzheimer’s Association; Alzheimer’s Drug Discovery Foundation; Araclon Biotech; BioClinica, Inc.; Biogen; Bristol-Myers Squibb Company; CereSpir, Inc.; Cogstate; Eisai Inc.; Elan Pharmaceuticals, Inc.; Eli Lilly and Company; EuroImmun; F. Hoffmann-La Roche Ltd and its affiliated company Genentech, Inc.; Fujirebio; GE Healthcare; IXICO Ltd.; Janssen Alzheimer Immunotherapy Research & Development, LLC.; Johnson & Johnson Pharmaceutical Research & Development LLC.; Lumosity; Lundbeck; Merck & Co., Inc.; Meso Scale Diagnostics, LLC.; NeuroRx Research; Neurotrack Technologies; Novartis Pharmaceuticals Corporation; Pfizer Inc.; Piramal Imaging; Servier; Takeda Pharmaceutical Company; and Transition Therapeutics. The Canadian Institutes of Health Research is providing funds to support ADNI clinical sites in Canada. Private sector contributions are facilitated by the Foundation for the National Institutes of Health (www.fnih.org). The grantee organization is the Northern California Institute for Research and Education, and the study is coordinated by the Alzheimer’s Therapeutic Research Institute at the University of Southern California. ADNI data are disseminated by the Laboratory for Neuro Imaging at the University of Southern California.

REFERENCES

[1] N. M. Bressler, "Age-Related Macular Degeneration Is the Leading Cause of Blindness," *JAMA*, vol. 291, no. 15, pp. 1900–1901, 04 2004.

[2] J. A. Hallak, L. de Sisternes, A. Osborne, B. Yaspan, D. L. Rubin, and T. Leng, "Imaging, genetic, and demographic factors associated with conversion to neovascular age-related macular degeneration: secondary analysis of a randomized clinical trial," *JAMA ophthalmology*, vol. 137, no. 7, pp. 738–744, 2019.

[3] Z. Breijyeh and R. Karaman, "Comprehensive review on alzheimer's disease: causes and treatment," *Molecules*, vol. 25, no. 24, p. 5789, 2020.

[4] M. Bucholc, S. Titarenko, X. Ding, C. Canavan, and T. Chen, "A hybrid machine learning approach for prediction of conversion from mild cognitive impairment to dementia," *Expert Systems with Applications*, vol. 217, p. 119541, 2023.

[5] K. Berg, T. R. Pedersen, L. Sandvik, and R. Bragadóttir, "Comparison of ranibizumab and bevacizumab for neovascular age-related macular degeneration according to lucas treat-and-extend protocol," *Ophthalmology*, vol. 122, no. 1, pp. 146–152, 2015.

[6] J. Yim *et al.*, "Predicting conversion to wet age-related macular degeneration using deep learning," *Nature Medicine*, vol. 26, no. 6, pp. 892–899, 2020.

[7] M. Ansart *et al.*, "Predicting the progression of mild cognitive impairment using machine learning: A systematic, quantitative and critical review," *Medical Image Analysis*, vol. 67, p. 101848, 2021.

[8] G. Bertasius, H. Wang, and L. Torresani, "Is space-time attention all you need for video understanding?" in *International Conference on Machine Learning*. PMLR, July 2021, pp. 813–824.

[9] S.-C. Huang, A. Pareek, M. Jensen, M. P. Lungren, S. Yeung, and A. S. Chaudhari, "Self-supervised learning for medical image classification: a systematic review and implementation guidelines," *NPJ Digital Medicine*, vol. 6, no. 1, p. 74, 2023.

[10] T. Emre, A. Chakravarty, D. Lachinov, A. Rivail, U. Schmidt-Erfurth, and H. Bogunović, "Learning temporally equivariance for degenerative disease progression in oct by predicting future representations," in *International Conference on Medical Image Computing and Computer-Assisted Intervention*. Springer, 2024, pp. 196–206.

[11] B. Dufumier *et al.*, "Contrastive learning with continuous proxy metadata for 3d mri classification," in *International Conference on Medical Image Computing and Computer-Assisted Intervention*. Springer, 2021, pp. 58–68.

[12] A. Rivail *et al.*, "Modeling disease progression in retinal octs with longitudinal self-supervised learning," in *International Workshop on PRedictive Intelligence In MEdicine*. Springer, 2019, pp. 44–52.

[13] M. Ren, N. Dey, M. Styner, K. Botteron, and G. Gerig, "Local spatiotemporal representation learning for longitudinally-consistent neuroimage analysis," *Advances in Neural Information Processing Systems*, vol. 35, pp. 13 541–13 556, 2022.

[14] T. Chen, S. Kornblith, M. Norouzi, and G. Hinton, "A simple framework for contrastive learning of visual representations," in *International Conference on Machine Learning*. PMLR, 2020, pp. 1597–1607.

[15] K. He, X. Chen, S. Xie, Y. Li, P. Dollár, and R. Girshick, "Masked autoencoders are scalable vision learners," in *Proceedings of the IEEE/CVF conference on computer vision and pattern recognition*, 2022, pp. 16 000–16 009.

[16] D. Pathak, P. Krahenbuhl, J. Donahue, T. Darrell, and A. A. Efros, "Context encoders: Feature learning by inpainting," in *Proceedings of the IEEE conference on computer vision and pattern recognition*, 2016, pp. 2536–2544.

[17] L. Kong *et al.*, "Understanding masked autoencoders via hierarchical latent variable models," in *Proceedings of the IEEE/CVF Conference on Computer Vision and Pattern Recognition*, 2023, pp. 7918–7928.

[18] Y. Zhou *et al.*, "A foundation model for generalizable disease detection from retinal images," *Nature*, vol. 622, no. 7981, pp. 156–163, 2023.

[19] J. Qiu *et al.*, "Development and validation of a multimodal multitask vision foundation model for generalist ophthalmic artificial intelligence," *NEJM AI*, vol. 1, no. 12, p. A10a2300221, 2024.

[20] C. Feichtenhofer, Y. Li, and K. He, "Masked autoencoders as spatiotemporal learners," *Advances in neural information processing systems*, vol. 35, pp. 35 946–35 958, 2022.

[21] Z. Tong, Y. Song, J. Wang, and L. Wang, "VideoMAE: Masked autoencoders are data-efficient learners for self-supervised video pre-training," in *Advances in Neural Information Processing Systems*, vol. 35, 2022, pp. 10 078–10 093.

[22] Q. Wu, T. Yang, Z. Liu, B. Wu, Y. Shan, and A. B. Chan, "Dropmae: Masked autoencoders with spatial-attention dropout for tracking tasks," in *Proceedings of the IEEE/CVF Conference on Computer Vision and Pattern Recognition*, 2023, pp. 14 561–14 571.

[23] J. Yang *et al.*, "Two-year risk of exudation in eyes with nonexudative age-related macular degeneration and subclinical neovascularization detected with swept source optical coherence tomography angiography," *American Journal of Ophthalmology*, vol. 208, pp. 1–11, 2019.

[24] Y. Zhang, C. Chen, S. Shit, S. Starck, D. Rueckert, and J. Pan, "Whole heart 3d+ t representation learning through sparse 2d cardiac mr images," in *International Conference on Medical Image Computing and Computer-Assisted Intervention*. Springer, 2024, pp. 359–369.

[25] R. Zeghlache *et al.*, "L-mae: Longitudinal masked auto-encoder with time and severity-aware encoding for diabetic retinopathy progression prediction," *Computers in Biology and Medicine*, vol. 185, p. 109508, 2025.

[26] A. Gupta, J. Wu, J. Deng, and F.-F. Li, "Siamese masked autoencoders," *Advances in Neural Information Processing Systems*, vol. 36, pp. 40 676–40 693, 2023.

[27] A. Eymaël, R. Vandeghen, A. Cioppa, S. Giancola, B. Ghanem, and M. Van Droogenbroeck, "Efficient image pre-training with siamese cropped masked autoencoders," in *European Conference on Computer Vision*. Springer, 2025, pp. 348–366.

[28] P. Weinzaepfel *et al.*, "Croco: Self-supervised pre-training for 3d vision tasks by cross-view completion," *Advances in Neural Information Processing Systems*, vol. 35, pp. 3502–3516, 2022.

[29] M. Tang, A. Cozma, K. Georgiou, and H. Qi, "Cross-scale mae: A tale of multiscale exploitation in remote sensing," *Advances in Neural Information Processing Systems*, vol. 36, pp. 20 054–20 066, 2023.

[30] S. Wang, V. Leroy, Y. Cabon, B. Chidlovskii, and J. Revaud, "Dust3r: Geometric 3d vision made easy," in *Proceedings of the IEEE/CVF Conference on Computer Vision and Pattern Recognition*, 2024, pp. 20 697–20 709.

[31] E. Denton and R. Fergus, "Stochastic video generation with a learned prior," in *International conference on machine learning*. PMLR, 2018, pp. 1174–1183.

[32] D. P. Kingma and M. Welling, "Auto-encoding variational bayes," 2013.

[33] M. Petrovich, M. J. Black, and G. Varol, "Action-conditioned 3d human motion synthesis with transformer vae," in *Proceedings of the IEEE/CVF International Conference on Computer Vision*, 2021, pp. 10 985–10 995.

[34] H. Jang, D. Kim, J. Kim, J. Shin, P. Abbeel, and Y. Seo, "Visual representation learning with stochastic frame prediction," in *International Conference on Machine Learning*. PMLR, 2024, pp. 21 289–21 305.

[35] D. Hafner, J. Pasukonis, J. Ba, and T. Lillicrap, "Mastering diverse domains through world models," *arXiv preprint arXiv:2301.04104*, 2023.

[36] D. Schmidt and M. Jiang, "Learning to act without actions," in *The Twelfth International Conference on Learning Representations*, 2024.

[37] V. Micheli, E. Alonso, and F. Fleuret, "Efficient world models with context-aware tokenization," in *International Conference on Machine Learning*. PMLR, 2024, pp. 35 623 – 35 638.

[38] A. Dosovitskiy *et al.*, "An image is worth 16x16 words: Transformers for image recognition at scale," in *International Conference on Learning Representations*, 2021.

[39] Z. Chen, D. Agarwal, K. Aggarwal, W. Safta, M. M. Balan, and K. Brown, "Masked image modeling advances 3d medical image analysis," in *Proceedings of the IEEE/CVF Winter Conference on Applications of Computer Vision*, 2023, pp. 1970–1980.

[40] K. Kunanbayev, V. Shen, and D.-S. Kim, "Training vit with limited data for alzheimer's disease classification: An empirical study," in *International Conference on Medical Image Computing and Computer-Assisted Intervention*. Springer, 2024, pp. 334–343.

[41] W. Peebles and S. Xie, "Scalable diffusion models with transformers," in *Proceedings of the IEEE/CVF International Conference on Computer Vision*, 2023, pp. 4195–4205.

[42] S. Elfwing, E. Uchibe, and K. Doya, "Sigmoid-weighted linear units for neural network function approximation in reinforcement learning," *Neural networks*, vol. 107, pp. 3–11, 2018.

[43] Y. Cong *et al.*, "Satmae: Pre-training transformers for temporal and multi-spectral satellite imagery," *Advances in Neural Information Processing Systems*, vol. 35, pp. 197–211, 2022.

[44] Y. Bengio, N. Léonard, and A. Courville, "Estimating or propagating gradients through stochastic neurons for conditional computation," *arXiv preprint arXiv:1308.3432*, 2013.

[45] D. P. Kingma, D. J. Rezende, S. Mohamed, and M. Welling, "Semi-supervised learning with deep generative models," *Advances in neural information processing systems*, vol. 27, p. 3581–3589, 2014.

- [46] M. Burchi and R. Timofte, “Accurate and efficient world modeling with masked latent transformers,” in *International Conference on Machine Learning*. PMLR, 2025.
- [47] J. Sutton *et al.*, “Developing and validating a multivariable prediction model which predicts progression of intermediate to late age-related macular degeneration—the pinnacle trial protocol,” *Eye*, vol. 37, no. 6, pp. 1275–1283, 2023.
- [48] R. C. Petersen *et al.*, “Alzheimer’s disease neuroimaging initiative (adni) clinical characterization,” *Neurology*, vol. 74, no. 3, pp. 201–209, 2010.
- [49] L. Puglisi, D. C. Alexander, and D. Ravi, “Enhancing spatiotemporal disease progression models via latent diffusion and prior knowledge,” in *International Conference on Medical Image Computing and Computer-Assisted Intervention*. Springer, 2024, pp. 173–183.
- [50] N. J. Tustison *et al.*, “N4itk: improved n3 bias correction,” *IEEE transactions on medical imaging*, vol. 29, no. 6, pp. 1310–1320, 2010.
- [51] A. Hoopes, J. S. Mora, A. V. Dalca, B. Fischl, and M. Hoffmann, “Synthstrip: skull-stripping for any brain image.” *NeuroImage*, vol. 260, p. 119474, 2022.
- [52] B. B. Avants, C. L. Epstein, M. Grossman, and J. C. Gee, “Symmetric diffeomorphic image registration with cross-correlation: evaluating automated labeling of elderly and neurodegenerative brain,” *Medical image analysis*, vol. 12, no. 1, pp. 26–41, 2008.
- [53] J. Carreira and A. Zisserman, “Quo vadis, action recognition? a new model and the kinetics dataset,” in *Proceedings of the IEEE/CVF Conference on Computer Vision and Pattern Recognition*, 2017, pp. 6299–6308.
- [54] I. Loshchilov and F. Hutter, “Decoupled weight decay regularization,” in *International Conference on Learning Representations*, 2019.
- [55] X. Chen *et al.*, “Context autoencoder for self-supervised representation learning,” *International Journal of Computer Vision*, vol. 132, no. 1, pp. 208–223, 2024.
- [56] A. El-Nouby *et al.*, “Scalable pre-training of large autoregressive image models,” in *International Conference on Machine Learning*. PMLR, 2024, pp. 12371–12384.